AGU PUBLICATIONS

JGR

Journal of Geophysical Research: Biogeosciences

RESEARCH ARTICLE
10.1002/2015JG003309

Key Points:
- Freshwater lake water column biogeochemistry and methane generation
- Shallow sediment biogeochemistry and microbiology
- Carbon turnover, stable isotopes, and seasonal methane flux

Supporting Information:
- Data Set S1
- Supporting Information S1

Correspondence to:
S. R. Parker,
sparker@mtech.edu

Citation:
Parker, S. R., R. F. West, E. S. Boyd, J. Feyhl-Buska, C. H. Gammons, T. B. Johnston, G. P. Williams, and S. R. Poulson (2016), Biogeochemical and microbial seasonal dynamics between water column and sediment processes in a productive mountain lake: Georgetown Lake, MT, USA, *J. Geophys. Res. Biogeosci.*, *121*, 2064–2081, doi:10.1002/2015JG003309.

Received 16 DEC 2015
Accepted 6 JUL 2016
Accepted article online 12 JUL 2016
Published online 8 AUG 2016

Biogeochemical and microbial seasonal dynamics between water column and sediment processes in a productive mountain lake: Georgetown Lake, MT, USA

Stephen R. Parker[1], Robert F. West[1], Eric S. Boyd[2,3], Jayme Feyhl-Buska[2], Christopher H. Gammons[4], Tyler B. Johnston[1], George P. Williams[1], and Simon R. Poulson[5]

[1]Department of Chemistry & Geochemistry, Montana Tech of The University of Montana, Butte, Montana, USA, [2]Department of Microbiology and Immunology, Montana State University, Bozeman, Montana, USA, [3]NASA Astrobiology Institute, Mountain View, California, USA, [4]Department of Geological Engineering, Montana Tech of The University of Montana, Butte, Montana, USA, [5]Department of Geological Sciences & Engineering, University of Nevada, Reno, Reno, Nevada, USA

Abstract This manuscript details investigations of a productive, mountain freshwater lake and examines the dynamic relationship between the chemical and stable isotopes and microbial composition of lake bed sediments with the geochemistry of the lake water column. A multidisciplinary approach was used in order to better understand the lake water-sediment interactions including quantification and sequencing of microbial 16S rRNA genes in a sediment core as well as stable isotope analysis of C, S, and N. One visit included the use of a pore water sampler to gain insight into the composition of dissolved solutes within the sediment matrix. Sediment cores showed a general decrease in total C with depth which included a decrease in the fraction of organic C combined with an increase in the fraction of inorganic C. One sediment core showed a maximum concentration of dissolved organic C, dissolved inorganic C, and dissolved methane in pore water at 4 cm depth which corresponded with a sharp increase in the abundance of 16S rRNA templates as a proxy for the microbial population size as well as the peak abundance of a sequence affiliated with a putative methanotroph. The isotopic separation between dissolved inorganic and dissolved organic carbon is consistent with largely aerobic microbial processes dominating the upper water column, while anaerobic microbial activity dominates the sediment bed. Using sediment core carbon concentrations, predictions were made regarding the breakdown and return of stored carbon per year from this temperate climate lake with as much as 1.3 Gg C yr^{-1} being released in the form of CO_2 and CH_4.

1. Introduction

Freshwater lakes are dynamic, "living" systems that are integral components of the global hydrological network and important resources for recreation, agricultural/industrial uses, and power generation. Natural and man-made lakes can be viewed as temporary water storage systems, and inputs such as nutrients, metals/metalloids, and organics can have severe impacts on limnological processes, biological productivity, and the quality of water within and leaving the lake. More specifically, the addition of excess nutrients to lakes can lead to eutrophication which in turn has the potential to amplify localized or wide spread anoxic conditions due to excessively high biological productivity (see review by *Smith and Schindler* [2009]). Lakes can also act as important storage compartments for carbon that is sequestered from the atmosphere into sediments as organic or inorganic carbon [*Einsele et al*., 2001; *Downing et al*., 2008; *Tranvik et al*., 2009; *Kastowski et al*., 2011].

There are approximately 3×10^8 natural lakes globally (4.2×10^6 km^2), the majority of which are <1 km^2 [*Downing et al*., 2006] such that about 0.3% of continental land is covered with freshwater lakes/reservoirs [*Downing et al*., 2006]. Lakes are important regulators of carbon cycling and are of similar influence to that of terrestrial ecosystem production [*Tranvik et al*., 2009]. Lakes can be significant sources of CH_4 to the atmosphere [*Rudd and Hamilton*, 1978; *Michmerhuizen et al*., 1996; *Utsumi et al*., 1998; *Bastviken et al*., 2004; *Schubert et al*., 2012]. CH_4 has about 21 times the radiative forcing of CO_2 over periods of 20 years [*Rodhe*, 1990]. By some estimates, the global flux of CH_4 released by lakes completely counteracts the beneficial consumption of CH_4 by upland soil methanotrophs and accounts for between 6 and 16% of the global methane load [*Bastviken et al*., 2004, 2011].

An important question in aquatic environments is whether oxygen is present or not (anoxia) since it has a major influence on redox potential and pH, which in turn control the mobility and reactivity of a host of

chemical species and which biogeochemical processes take place in a given system [*Stumm and Morgan*, 1996; *Jones and Mulholland*, 2000]. Shallow lakes, common in boreal and temperate climates [*Downing et al*., 2006], are especially vulnerable to eutrophication due to anthropogenic activities. Eutrophication can in some cases lead to severe anoxia and potentially a "catastrophic shift" in the lake ecosystem [*Scheffer et al*., 2001; *Moss et al*., 2011].

Here we present an examination of recent results that illustrate the conditions supporting severe anoxia and methane fluxes from Georgetown Lake (GTL), Montana, USA. These results include a molecular analysis of microbial communities found in lake bed sediments in relation to the geochemical composition within those sediments. Previous work at Georgetown Lake identified seasonal anoxic conditions near the bottom with stratification that takes place during periods of ice cover [*Gammons et al*., 2014]. These conditions contributed to accumulations of reduced species such as CH_4, H_2S, and NH_4^+ in the anoxic zone (bottom 1.5–3 m). Additionally, the $\delta^{13}C$ composition of sediments (solids and pore water) in comparison to that of the water column was used to determine the major processes influencing lake biogeochemistry. This manuscript details the interrelationships between the shallow sediment and water column biogeochemistry and its connection to the seasonal biogeochemical dynamics of the lacustrine system, including the release of CH_4 to the atmosphere.

2. Site Description

Georgetown Lake (GTL) is located in southwestern Montana (MT) approximately 37 km west of Anaconda, MT, at an elevation of 1690 m above sea level, is mostly surrounded by the mountains of the Pintlar and Flint Creek ranges, and has a surface area of about 1.2 km^2 (Figure 1). GTL is fed from the east and south by water from the North Fork of Flint Creek (NFF), several springs along the lakeshore (Emily's Spring, ES; Stuart Mill Spring, SMS) and an aqueduct from Silver Lake to the southeast. There are also several submerged springs along the east shore [*U.S. Environmental Protection Agency* (*EPA*), 1976; *Shaw et al*., 2013]. Originally used as a grazing pasture [*Knight et al*., 1976], the Montana Power Company built a dam across Flint Creek in 1885 to supply power to local mining operations, creating GTL. Currently, GTL serves as an important recreational body of water in southwestern Montana, with numerous seasonal and full-time residences around the lake, fishing access sites, and campgrounds.

Studies in the 1970s classified GTL as a eutrophic lake based upon excess nutrient loading [*U.S. EPA*, 1976]. Other studies have described severe anoxic conditions during winter ice cover [*Knight et al*., 1976; *U.S. EPA*, 1976; *Knight*, 1981; *Trabert*, 1993; *Henne*, 2011; *Johnston*, 2014], and winter fish kills have been reported as well. A more recent report from a multiyear study found GTL becoming less eutrophic based on lowering nutrient concentrations [*Stafford*, 2013]. However, this report also recorded the persistence of severe anoxic zones under ice cover as well as large-scale blooms of white-stemmed pondweed (*Potamogeton praelongus*) and *Chara* sp. (stem-like, multicellular green algae) during the ice-free season. These blooms add large amounts of biomass to the sediments which may continue to fuel the oxygen depletion during winter months.

Sampling locations (Figure 1) included the GT2 site (46°10.895'N, 113°18.755'W) [see *Gammons et al*., 2014] and sites designated RB1 (46°12.415'N, 113°16.579'W), PB1 (46°11.914'N, 113°17.527'W), and SM1 (46° 10.777'N, 113°16.646'W). The RB1 site is near the dam, PB1 is near Piney Campground in Rainbow Bay, and SM1 is in the southern part of the lake near a bay fed by Stuart Mill Spring. GT2 is in Badger Bay, the largest bay on the west side of the lake.

Further details of the limnology, geology, and geochemistry of GTL can be found in *Knight et al*. [1976], *U.S. EPA* [1976], *Knight* [1981], *Garrett* [1983], *Trabert* [1993], *Henne* [2011], *Stafford* [2013], *Johnston* [2014], and *Gammons et al*. [2014].

3. Methods

3.1. Field Methods

Results presented here include data from 11 site visits to GTL starting in September 2013 through March 2015. Winter sampling events took place using holes augured through the ice, and during open water a boat was used. Sample water was pumped using a peristaltic pump, and the lines were purged for 10+ min at each

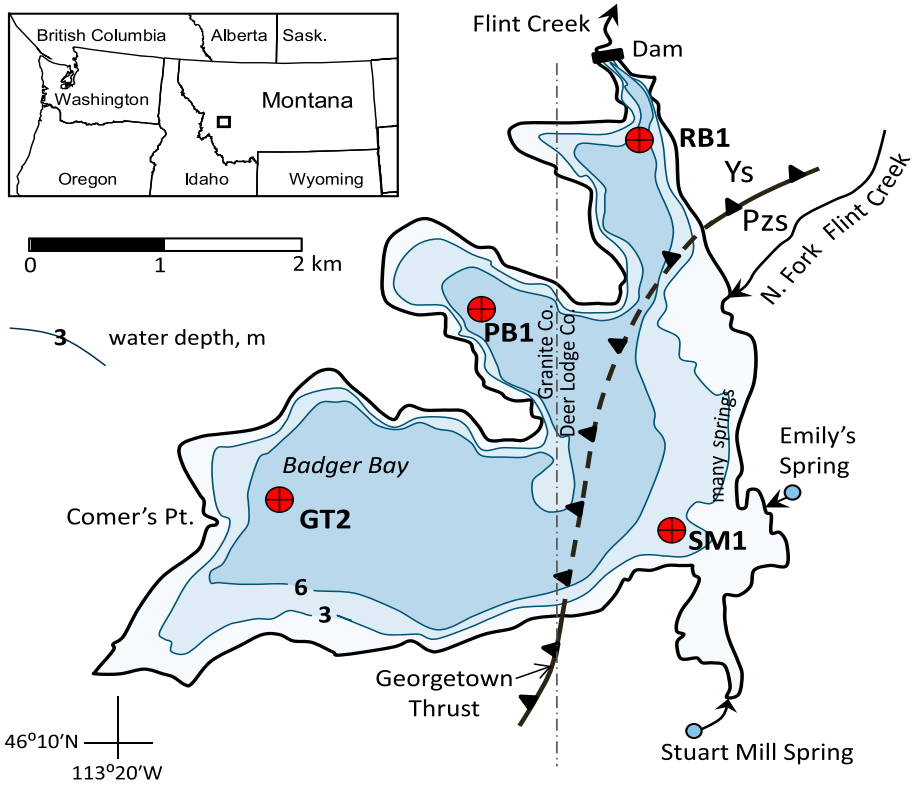

Figure 1. Location map (adapted from *Gammons et al.* [2014]) showing the RB1, GT2, PB1, and SM1 sampling sites reported here. Also shown are the major surface water sources: N. Fork of Flint Creek, Emily's Spring, and Stuart Mill Spring. Contours show depth (meters) of water at full pool. A thrust fault divides the lake, with triangles on the upthrust side. Ys = Mid-Proterozoic carbonate and siliclastic rocks of the Belt Supergroup; Pzs = Paleozoic sediments, undivided (includes Mississippian Madison Group limestone). Color on all figures is available in the online version.

depth. An MS-5 Hydrolab was attached to the end of the pump tubing as it was lowered to each sampling depth, and pH, temperature (°C), specific conductivity (SC, μS/cm), oxidation-reduction potential (ORP or Eh versus SHE, mV), and dissolved oxygen (DO, mg/L and % sat) were recorded from a meter at the surface. The MS-5 was calibrated within 1–2 h before each sampling event using standard pH buffers, standard KCl solutions for SC, Zobell's solution for Eh, and air saturated water for the luminescent DO probe. Both unfiltered and filtered (0.2 μm polyethersulfone (PES) filters) water samples were taken. Samples were collected for dissolved inorganic carbon (DIC, mg L^{-1}), dissolved organic carbon (DOC, mg L^{-1}), dissolved anions (ion chromatography), dissolved cations (inductively coupled plasma optical emission spectroscopy (ICP-OES)), total sulfide ($S^{2-} + HS^- + H_2S$; mg S L^{-1}), total suspended solids (TSS, milligram suspended sediment per kilogram water), total ammonia ($NH_3 + NH_4^+$; mg N L^{-1}), alkalinity (as mg $CaCO_3$ L^{-1}), stable C isotopes of DOC and DIC ($\delta^{13}C_{DIC}$, $\delta^{13}C_{DOC}$), and stable isotopes of water ($\delta^{18}O_{H2O}$ and δD_{H2O}). Samples for sulfide analysis were treated in the field with the reagents for later colorimetric analysis (described below). Unfiltered samples were also collected for determination of dissolved CH_4 concentration in sealed septum capped vials with no head space. All samples were stored on ice and refrigerated upon returning to the laboratory. Samples for cation analysis were acidified to 1% (v/v) with trace metal grade HNO_3. On six separate visits shallow sediment cores were collected using a stainless steel coring device with a clear plastic insert that was 4.8 cm in diameter. Cores collected, generally ranged from 10 to 17 cm in length, were stored on ice in the field and frozen after returning to the laboratory. During several field visits 500–1000 mL of water was collected for measurement of total suspended solids (TSS). This water was kept refrigerated, weighed, and then filtered in the laboratory on preweighed fiberglass filters (mass reproducible to ± 0.001 g). The filters with suspended solids were dried at 50°C and reweighed. Some of these filters with imbedded material were later used to determine the $\delta^{13}C$ of total particulate carbon (TPC) (described below). In most cases at least one replicate sample was collected as part of each analyte set. Analytical work was repeated if the replicate samples did not agree within 5%.

The supporting information includes field records and analytical results of all samples collected during site visits. Additional details of field methods are similar to those found in *Gammons et al.* [2014].

3.2. Pore Water Sampling

A pore water sampler ("peeper"; Rickly Hydrological) [after *Hesslein*, 1976] was used to sample sediment pore water by diffusion into cells that were prefilled with deoxygenated, deionized water, covered by a permeable nylon membrane (5 μm pore size) and then kept submerged in deionized water that had Ar continuously bubbled through to maintain the oxygen-free condition [see *Shaw et al.*, 2013]. The peeper was installed through a hole drilled in the ice in approximately 6.1 m of water on 1 March 2015 (pictures in the supporting information). Detachable 2.6 cm diameter PVC pipes in 1.5 m sections were used to lower the sampler to the bottom, and then the pipe was slowly "rocked" side to side as the sampler was inserted into the sediment (~14 cm deep). A light rope was attached to the peeper as it was lowered into the lake. After being inserted in the bottom sediment the insertion pipe was unscrewed and removed from the water with the rope remaining on top of the ice and tied to a brace that spanned the hole through the ice. The peeper was retrieved on 16 March by pulling it up with the rope. The peeper was immediately placed in a large clear plastic bag that was sealed at the top and had a tube inserted from an Ar tank so that it could be purged and kept oxygen free. Water samples were collected from the peeper cells by inserting a syringe needle through the plastic bag and peeper membrane, drawing the cell contents up into the syringe and then dispensing into the appropriate sample bottle. Dilutions were made in the field with degassed deionized water, and all masses of samples and reagents were recorded to calculate dilution factors. All samples were kept on ice and then refrigerated after returning to the lab.

3.3. Analytical Methods

DIC and DOC concentrations and C isotope composition of aqueous samples (DIC, DOC, $\delta^{13}C_{DIC}$, and $\delta^{13}C_{DOC}$) were determined using an Aurora 1030 W TIC/TOC analyzer interfaced with a Picarro G2131-i carbon isotope analyzer. A Costech combustion module was used for $\delta^{13}C$ of solid samples in conjunction with the Picarro G2131-i. Carbon isotopic analysis was calibrated using the standards USGS 40 (glutamic acid, $\delta^{13}C = -26.39$), USGS 41 (enriched glutamic acid, $\delta^{13}C = +37.63$), NBS 18 (calcite, $\delta^{13}C = -5.014$), and CH-6 (sucrose, $\delta^{13}C = -10.449$) as well as standardized reference material (Li_2CO_3 and $NaHCO_3$ for inorganic C; sucrose and potassium hydrogen phthalate (KHP; $KC_8H_5O_4$) for organic C). Isotopic analysis for water at Montana Tech used a Picarro L1102-i CRDS water isotope analyzer for $\delta^{18}O_{H2O}$ and δD_{H2O} and was calibrated using isotopic standards USGS 47 ($\delta^{18}O = -19.8$; $\delta D = -150.2$), USGS 48 ($\delta^{18}O = -2.224$; $\delta D = -2.0$), and Vienna SMOW (VSMOW) ($\delta^{18}O = 0.0$; $\delta D = 0.0$). All C, H, and O isotope values are reported in units of per mil (‰) in the usual δ notation versus VSMOW for oxygen and hydrogen and VPDB for C. Replicate analyses indicated a relative error of ± 0.1‰ for $\delta^{18}O_{H2O}$, ± 1‰ for δD_{H2O}, and ± 0.05‰ for $\delta^{13}C_{DIC}$ and $\delta^{13}C_{DOC}$.

Sediment cores were partially thawed and segmented into 1–2 cm sections which were then dried at 70°C for 48–72 h before being crushed and screened (100 mesh) to a fine powder. Approximately 0.5 g of each sediment section was treated with 5 mL of 10% HCl, reacted at room temperature for 24 h, and then dried in an oven at 70°C for 24 to 48 h. The untreated and acid-treated fine sediment materials were analyzed for the mass of carbon and $\delta^{13}C$ per sample. The mass of C in each sample was determined based on the relationship between the total CO_2 peak area obtained during Picarro analysis and mass of C in the standards. Acid-treated samples were used to determine the $\delta^{13}C_{Org}$ of organic carbon and organic C mass in each sample. The mass of inorganic C in each sample was determined by the difference between the acid-treated and untreated samples. The fraction of inorganic and organic C in each sample was used along with $\delta^{13}C_{Org}$ to determine $\delta^{13}C_{Inorg}$ using the following isotopic mass balance relationship (equation (1)):

$$\delta^{13}C_{Tot} = \delta^{13}C_{Org}\cdot\text{frac org} + \delta^{13}C_{Inorg}\cdot\text{frac inorg}$$
$$\delta^{13}C_{Inorg} = \frac{\left(\delta^{13}C_{Tot} - \delta^{13}C_{Org}\cdot\text{frac org}\right)}{\text{frac inorg}} \quad (1)$$

Material collected on the TSS filters was used to determine $\delta^{13}C$ of total particulate carbon (TPC). A piece of the fiberglass filter with embedded particulate material was placed in the Sn cup used for the CM-CRDS analysis as described above. Fiberglass filter material analyzed by itself (to account for interference) did not produce enough CO_2 to be measurable.

Sediment samples from the May 2014 core were sent to Energy Labs (Billings, MT) for determination of total N, S, and P. Sediment cores collected in July 2014 were digested at Montana Tech by several methods to determine element compositions. Digestions for determination of elemental compositions followed the method of *Borg and Jonsson* [1996] using ~0.5 g sediment with 20 mL 7 M HNO_3 in autoclavable bottles (120°C; 60 min) which were followed by further digestion with H_2O_2. Digestion of sediments from the May 2014 core for the determination of $\delta^{34}S$ followed the method of *Gaudino et al*. [2007] using aqua regia (HNO_3 + HCl) with H_2O_2 in an autoclave. The liquid after digestion was filtered to remove fine particulates, and then 2 mL of a saturated $BaCl_2$ solution was added to precipitate $BaSO_4$. The white precipitate was collected as a slurry rinsed several times with deionized water and dried before being sent to the Stable Isotope Lab at the Univ. Nevada-Reno for $\delta^{34}S$ determination. Samples from the May 2014 core were also analyzed for $\delta^{15}N$. The analyses were performed using a Eurovector EA 3000 elemental analyzer interfaced to a Micromass IsoPrime stable isotope ratio mass spectrometer. Nitrogen isotope analyses were performed after the method described by *Werner et al*. [1999]. $\delta^{15}N$ results are reported in units of per mil versus air, with an approximate uncertainty of ±0.2‰. Sulfur isotope analyses were performed after the methods of *Giesemann et al*. [1994] and *Grassineau et al*. [2001]. V_2O_5 was added to $BaSO_4$ samples as a combustion aid, and the $\delta^{34}S$ results are reported in units of per mil versus VCDT, with a recommended uncertainty of ±0.2‰.

Analysis of CH_4 concentrations in water samples utilized an Aurora carbon analyzer (1030 W) in conjunction with a Picarro G-2131-i C-stable isotope analyzer. The Picarro instrument measures CH_4 concentration spectroscopically in order to correct for interference to the CO_2 measurement for determination of the relative concentrations of $^{12}CO_2$ versus $^{13}CO_2$. Reference solutions for calibration were generated by bubbling CH_4 through water in a closed vial to produce a saturated solution. The concentration of this solution was calculated based on the known solubility of CH_4 [*Wiesenburg and Guinasso*, 1979]. Several dilutions of the saturated solution were used to develop a calibration curve. Estimated error, based on duplicate determinations, was less than 2%.

Alkalinity titrations were performed in the lab using 100.0 mL of unfiltered sample, bromocresol green-methyl red indicator, and 1.600 N sulfuric acid. Total ammonia was determined using Hach method 8038 (detection limit 0.06 mg N-NH_3 L^{-1}) on 25 mL of filtered sample water. Total sulfide was determined using 25 mL of unfiltered water that was treated in field with Hach sulfide reagents to stabilize the sample then analyzed for sulfide concentrations in the lab using Hach method 8131 (detection limit 0.01 mg S L^{-1}). Concentrated samples often required a 5:1 dilution to avoid overrange concentrations for the colorimetric method. Soluble reactive phosphorous concentrations were determined within 12 h of collection using HACH method 8038 (detection limit 1.4 μM). Filtered unacidified samples were collected for major anions (fluoride, sulfate, nitrite, nitrate, chloride, bromide, and phosphate) analysis by Ion Chromatography ((EPA) method 300.0) at Montana Tech. Water samples and digestions of sediments were analyzed for major and trace elements by ICP-OES in the Montana Bureau of Mines and Geology lab at Montana Tech (EPA Method 200.7).

The partial pressure of dissolved CO_2 (pCO_2) in the water column was calculated using temperature, pH, alkalinity or total DIC, and depth with the program CO2-SYS [*Lewis and Wallace*, 1998].

3.4. Microbiological Methods

A single 13 cm long frozen (−80°C initially) sediment core sampled on 16 March 2015 was transferred to a cold lab (−20°C) at Montana State University where it was sectioned into 1 cm cylinders (13 in total) using a flame sterilized hack saw. Samples were maintained frozen during the entire cutting process. Frozen sediment segments were thawed in sterile petri dishes at room temperature in a laminar flow hood. The outer layer of sediment was gently removed to eliminate any contaminate materials from sample handling by briefly submerging a partially thawed segment in a second petri dish containing molecular grade H_2O. Two small aliquots (~250 mg wet weight) of each segment were transferred to sterile bead beating tubes supplied with the FastDNASpin Kit for Soil (MP Biomedicals).

Genomic DNA was extracted from sediments using a combined mechanical and chemical lysis protocol using the FastDNASpin Kit for Soil as previously described [*Boyd et al*., 2007]. Equal volumes of each extract were pooled, and genomic DNA in the pooled extract was quantified using the Qubit dsDNA HS Assay kit (Life Technologies, Grand Island, NY) and a Qubit 2.0 Fluorometer (Life Technologies). Thirty-five cycles of

polymerase chain reaction (PCR) were conducted with ~10 ng of genomic DNA as template using universal 16S rRNA gene primers 515 F (5′-GTGCCAGCMGCCGCGGTAA-3′) and 806R (5′-GGACTACHVGGGTWTCTAAT-3′) with reaction and cycling conditions as previously described [*Boyd et al*., 2007] and an annealing temperature of 54°C. PCR products were purified, quantified, and subjected to IonTorrent sequencing by Molecular Research, LLC, as previously described [*Hamilton et al*., 2013].

A total of 592,532 reads was obtained by multiplexed sequencing of 16S rRNA gene amplicons from the 13 sediment core depth intervals sampled. Post sequencing processing was performed with Mothur (version 1.29.2) [*Schloss et al*., 2009] as previously described [*Hamilton et al*., 2013]. Briefly, raw libraries were trimmed to a maximum length of 250 bases, filtered, and trimmed using a defined start site and an optimized end site based on inclusion of 85% of the total sequences. Chimeras were identified and removed using UCHIME [*Edgar et al*., 2011], and operational taxonomic units (OTUs) were assigned at a sequence similarity of 0.97 using the nearest-neighbor method. The remaining sequences were randomly subsampled resulting in 16,030 16S rRNA gene sequences per depth interval sampled. Sequences were classified using the Bayesian classifier (5) and the RDP database, with manual verification using BLASTn. The taxonomic affiliation of the five most abundant OTUs, which when combined reflected 54.5% to 73.7% of total sequences, was determined using maximum likelihood phylogenetic reconstructions with reference sequences compiled from GenBank using default settings within the program MEGA 6 [*Tamura et al*., 2013]. In addition, all reads classified within the archaeal domain and which were $>$0.1% of the total abundance of sequences for any library were further scrutinized to determine if they could be attributed to methanogen taxa. Raw untrimmed sequence and quality score files along with a mapping file have been deposited in the NCBI SRA database (accession number SRA315175).

A Bray Curtis distance matrix was calculated from OTU data using PAST (version 3) [*Hammer et al*., 2001]. PAST was also used to calculate a dendogram depicting the dissimilarity in the communities using this matrix. The Unweighted Pair Group Method with Arithmetic Mean (UPGMA) paired method was used to generate the dendogram, which was bootstrapped 100 times.

Quantitative PCR (qPCR) was used to estimate the number of 16S rRNA gene templates per unit dry mass (sediments) following previously developed methods [*Boyd et al*., 2011]. Two 16S rRNA gene clones, generated as previously described [*Boyd et al*., 2007], were used to create standard curves to relate template copy number to the threshold qPCR amplification signal. Estimates of the abundance of 16S rRNA genes from these two clones, when they were used in generating the standard curves, varied by less than a factor of 1.0 and thus were averaged for use in calculating the average template abundances and standard deviation in template abundances from replicate qPCRs. A standard curve was generated, as previously described [*Boyd et al*., 2011], over 6 orders of magnitude from 4.6×10^3 to 4.6×10^9 copies of template (Pearson $R^2 = 0.999$). qPCR assays were performed in a CFX Connect quantitative real-time PCR machine (Bio-Rad Laboratories, Hercules, California) in 0.5 mL optically clear PCR tubes using a SsoAdvanced Universal SYBR Green Supermix qPCR Kit (Bio-Rad Laboratories). qPCR assays were performed in a CFX Connect quantitative real-time PCR machine (Bio-Rad Laboratories, Hercules, California) in 0.5 mL optically clear PCR tubes (Bio-Rad Laboratories) using a SsoAdvanced Universal SYBR Green Supermix qPCR Kit. qPCR cycling conditions were as follows: an initial denaturing step at 98°C for 30 s followed by 35 cycles of 98°C for 30 s, specific annealing and elongation temperature for 1 min, and eventually a melt curve of 65–95°C in 5 s/0.5°C step increments. Specificity of the qPCR assays was verified by melt curve analysis. Negative control assays were performed in the absence of template DNA. Each assay was performed in triplicate, and the reported template abundances are the average and standard deviation of triplicate reactions for each DNA extract.

4. Results

4.1. Water Column Profiles

The CH_4 concentration, pH, DO, and SC were recorded near the bottom of the water column during all the sampling visits discussed in this manuscript and are summarized in Table 1. During some visits surface water sites around GTL (Figure 1) were also sampled including the North Fork of Flint Creek (NFF), Emily's Spring (ES), and Stuart Mill Spring (SMS) and are included here for comparison with lake samples.

Data from May 2014 (Figure 2), after 6 months of ice cover, and June 2014 (Figure 3; open water) are shown here for comparison of these different conditions (all field and laboratory data are included in the supporting information). Changes in water column chemistry near the bottom of the lake under ice included

Table 1. Summary of Basic Parameters Near the Sediment-Water Interface Plus Several Water Sources to GTL at Sites Sampled Showing Depth From Water Surface to Bottom, CH_4 Concentration, Temperature, pH (SU), Specific Conductivity (SC), and Dissolved Oxygen (DO) Concentration[a]

Site	Date	Depth (m)	CH_4 (μM)	Temp (°C)	pH	SC (µS/cm)	DO (mg/L)	Condition
GT-2	14 Dec 2013	5.9	20	3.6	7.64	218	4.6	ice
GT-2	26 Jan 2014	5.8	595	4.4	6.96	288	<0.05	ice
GT-2	28 Mar 2014	5.2	958	4.7	6.89	361	<0.05	ice
GT-2	8 May 2014	5.9	1940	5.2	6.69	489	<0.05	ice
RB-1	12 Jun 2014	3.6	101	14.2	7.94	211	8.3	OW
PB-1	12 Jun 2014	6.1	49	13.8	7.82	213	7.7	OW
GT-2	12 Jun 2014	6.1	37	14.3	8.08	220	8.1	OW
SM-1	12 Jun 2014	5.5	21	18.8	8.04	216	8.4	OW
RB-1	31 Jul 2014	3.6	34	19.3	8.78	194	9.0	OW
GT-2	31 Jul 2014	6.4	28	18.6	8.14	202	7.9	OW
SM-1	31 Jul 2014	5.5	28	18.8	8.75	192	10.0	OW
NFF	31 Jul 2014	surface	35	NA	NA	NA	NA	OW
ES	31 Jul 2014	surface	15	NA	NA	NA	NA	OW
SMS	31 Jul 2014	surface	15	NA	NA	NA	NA	OW
RB-1	7 Sep 2014	3.6	8.9	15.1	8.36	180	8.8	OW
GT-2	7 Sep 2014	6.4	10.5	15.0	8.46	181	8.7	OW
SM-1	7 Sep 2014	4.9	10.0	14.9	8.53	181	9.5	OW
NFF	7 Sep 2014	surface	NA	8.8	7.71	275	9.2	OW
ES	7 Sep 2014	surface	<3	9.1	7.11	275	6.0	OW
SMS	7 Sep 2014	surface	<3	6.0	7.41	241	10.0	OW
GT-2	16 Mar 2015	6.1	982	5.3	6.69	327	<0.05	ice

[a]RB1, PB1, GT2, and SM1 are lake sampling sites discussed in text. The North Fork of Flint Creek (NFF), Emily Spring (ES), and Stuart Mill Spring (SMS) are the major surface water sources to GTL (see Figure 1). OW = open water, NA = not available.

a decrease in pH resulting from increasing pCO_2 and a decrease in DO to values below detection (<0.1 mg L^{-1}, Figure 2). Total S^{2-} concentration increased with depth at the same time that SO_4^{2-} concentration decreased in the bottom ~1.5 m. Water column profiles from four sites measured on June 14, approximately 3 weeks after ice off, showed well-mixed profiles for all parameters from the surface to bottom (Figure 3).

A CH_4 concentration of 1.9 mM was recorded near the lake bottom at GT2 on 8 May 2014, while about 1 month later (12 June 2014) the concentrations of CH_4 at GT2, RB1, PB1, and SM1 were 37, 101, 49, and 21 μM, respectively (Table 1). Seasonal fluxes of CH_4 at the GT2 site will be summarized in section 5.1.

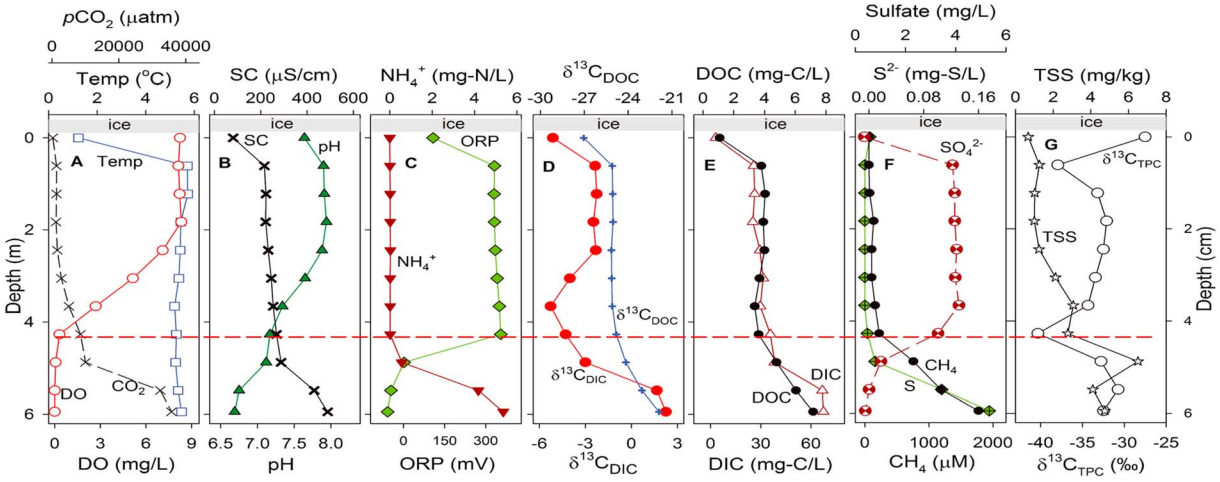

Figure 2. Vertical water column profiles for 8 May 2014 showing physical, chemical, and stable isotope values recorded approximately every 0.6 m to a depth near the sediment interface at ~6 m under ice: (A) Dissolved oxygen (DO), temperature, and pCO_2; (B) pH and SC; (C) ORP (Eh versus SHE, mV) and total NH_3; (D) $\delta^{13}C_{DOC}$ and $\delta^{13}C_{DIC}$ (E) DIC and DOC; (F) CH_4, sulfide, and sulfate; and (G) $\delta^{13}C_{TPC}$ and TSS. Ice was approximately 46 cm thick. The horizontal dashed line (red) shows the approximated location of the chemocline based on change in ORP and DO.

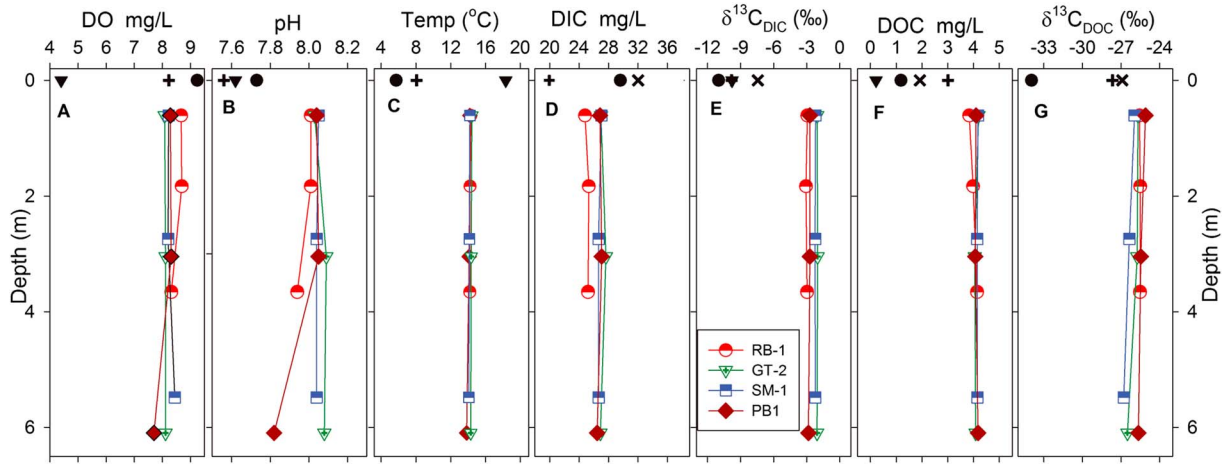

Figure 3. Vertical water column profile for 12 June 2014 (open water) showing physical, chemical, and stable isotope values recorded near surface, middepth, and near bottom at four sites: (A) DO, (B) pH, (C) temperature (°C), (D) DIC, (E) $\delta^{13}C_{DIC}$, (F) DOC, and (G) $\delta^{13}C_{DOC}$. Surface water sites near GTL are shown: Flint Creek below dam (cross), N. Fork Flint Creek (NFF, plus), Emily's Spring (ES, inverted triangle), and Stuart Mill Spring (SMS, circle).

Total suspended solids (TSS) collected in May 2014 ranged from 0.7 to 6.5 mg kg^{-1}, and total particulate carbon (TPC) in the TSS had $\delta^{13}C_{TPC}$ from −40.3 to −27.5‰ (Figure 2G). The concentration of TSS increased just below the chemocline boundary (where DO approached 0), and the $\delta^{13}C_{TPC}$ became isotopically lighter above the boundary and returned to heavier values below the boundary which will be discussed further below.

Vertical water column profiles from July 2014 and September 2014 were similar to June and showed a well-mixed water column (see supporting information). The deeper site (GT2) on July 2014 showed evidence of a weak hypolimnion with DO near the bottom dropping to about 4 mg L^{-1} (supporting information Figure S2).

During all water column samplings NO_3^- and PO_4^{3-} were below detection by conventional ion chromatography (<0.01 mg N L^{-1} and <0.02 mg P L^{-1}). *Gammons et al.* [2014] reported 0.5 μ*M* soluble reactive phosphorous (0.015 mg P L^{-1}) near the sediment-water interface at the GT2 site during ice cover.

4.2. Sediment Profiles

Shallow sediment cores (10–17 cm) were collected during site visits on September 2013, December 2013, January 2014, May 2014, July 2014, and March 2015. Representative results are presented here for sediment cores collected on May 2014 (ice cover, GT2, Figure 4), July 2014 (open water, three sites, Figure 5), and March 2015 (ice cover, GT2, Tables 2A–2C). The general trend in all sediment profiles was decreasing total C

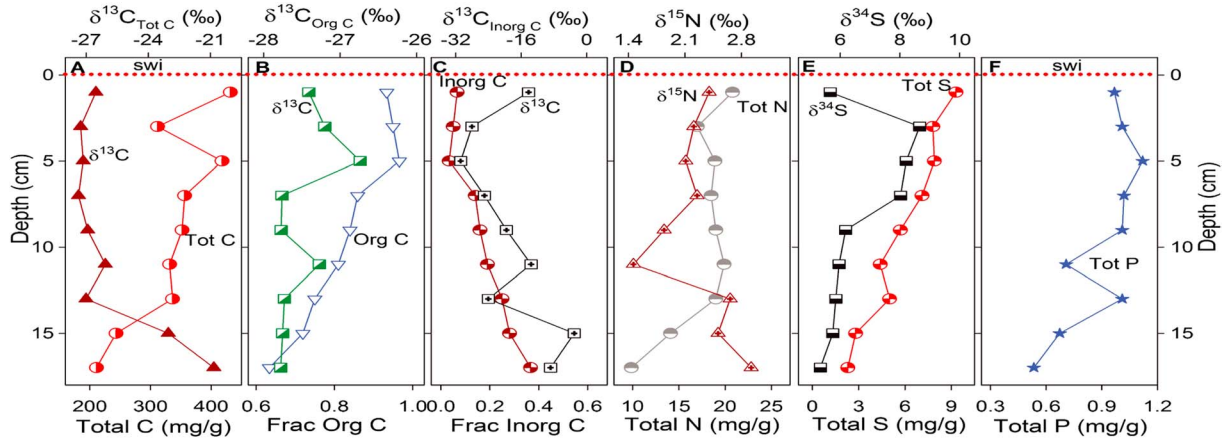

Figure 4. Sediment profiles from the GT2 site at GTL collected on 8 May 2014; (A) and $\delta^{13}C_{Tot}$, (B) fraction of organic C, $\delta^{13}C_{Org\ C}$, (C) fraction of inorganic C, $\delta^{13}C_{Inorg\ C}$, (D), $\delta^{15}N_{Tot}$, (E) $\delta^{34}S_{Tot}$, and (F) Total P. The sediment-water interface (swi) is shown by the dotted line (red).

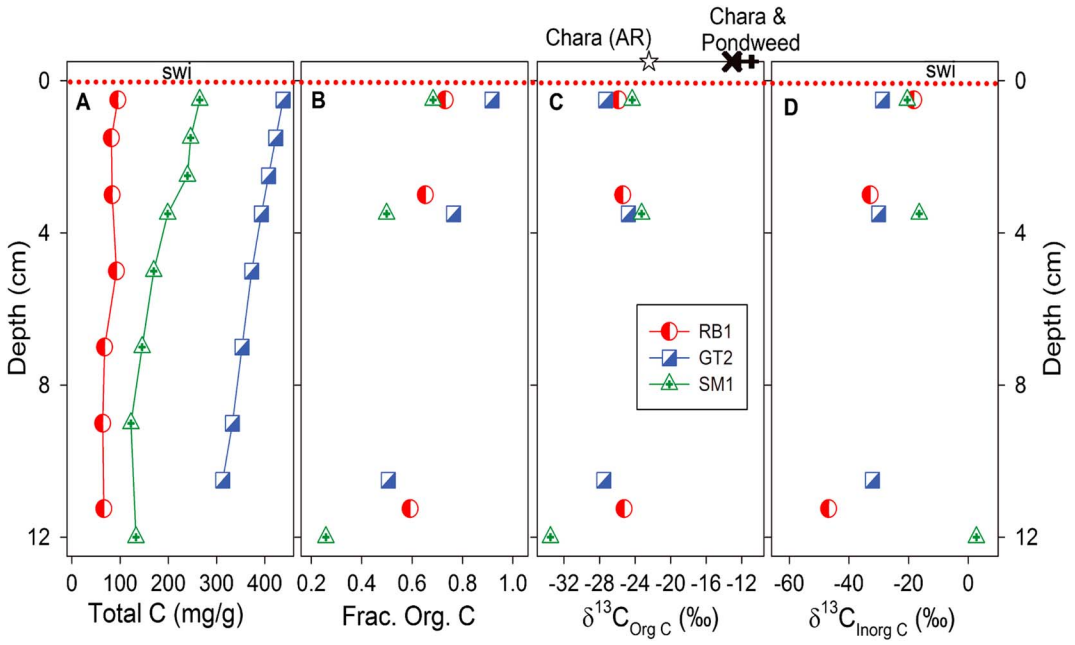

Figure 5. Sediment profiles from three sites at GTL collected on 31 July 2014: (A) total C, (B) fraction of organic C, (C) $\delta^{13}C_{Org\ C}$, and (D) $\delta^{13}C_{Inorg\ C}$. The sediment-water interface (swi) is shown by the dotted line (red). $\delta^{13}C$ values are shown for samples of *Chara* sp. (cross) and white-stemmed pondweed (plus) collected at this time as well as *Chara* that had been acid rinsed (star, AR) prior to analysis.

concentration with depth into the sediments accompanied by a decrease in the fraction of organic C with depth (Figures 4B, 5B and Tables 2A–2C). Sediment cores collected at three sites on July 2014 show a variation in the total C concentration (Figure 5A). The RB1 site near the dam on the easternside had the lowest total C concentration and a sandy texture. Sediment cores collected at the other sites had a dark, organic appearance of fine mud with a higher C content.

Values of $\delta^{13}C_{Org\ C}$ of the sediments ranged from −33.5 to −27.2‰, while $\delta^{13}C_{Inorg\ C}$ showed a much broader variation from −46.8 to +2.7‰. The highly depleted values occurred in clay-rich sediment near the bottom of the cores which is assumed to represent prereservoir wetland substrate. The lower core segments had a higher fraction of inorganic C than the upper segments and often had a visible reaction with HCl (effervescence) indicating the presence of carbonate minerals. These lower core segments also had the highest Ca concentration found in the sediments consistent with presence of $CaCO_3$ (data in the supporting information). Sediment samples collected in May 2014 were digested and analyzed for total N, S, and P. Total N showed a small decrease in the first 3 cm (21 to 17 mg g^{-1}) and then was relatively constant until about 15 cm when it decreased substantially to about 9.8 mg g^{-1} at 17 cm depth (Figure 4D). Total S decreased

Table 2A. Summary of Concentrations of Selected Analytes From Samples Collected on 16 March 2015 From the Water Column[a]

Depth (m)	Ba	Ca	Fe	K	Mg	Mn	Na	Si	Sr	SO_4^{2-}	$NH_3 + NH_4^+$-N	$\delta^{18}O_{H2O}$ (‰)	δD_{H2O} (‰)
0.9	NA	NA	NA	NA	NA	NA	NA	NA	NA	4.6	0.02	−13.9	−118.3
1.5	NA	NA	NA	NA	NA	NA	NA	NA	NA	4.6	0.05	−13.9	−117.4
2.1	NA	NA	NA	NA	NA	NA	NA	NA	NA	4.4	bd	−13.8	−116.4
2.7	0.04	29.0	0.07	1.4	12.3	NA	1.7	3.2	0.05	4.3	bd	−13.9	−117.1
3.4	0.04	29.8	bd	1.6	12.5	NA	2.1	3.2	0.05	4.5	bd	−13.8	−116.8
4.0	0.05	33.1	bd	1.5	12.7	NA	1.9	4.2	0.05	3.9	0.01	−13.9	−117.1
4.6	0.05	34.4	bd	1.8	12.7	0.64	1.9	4.5	0.06	3.6	0.14	−13.9	−117.5
5.2	0.06	35.4	0.04	1.9	12.6	0.89	1.8	4.7	0.06	1.6	0.42	−13.9	−117.2
5.8	0.06	38.3	0.07	2.1	12.6	0.47	1.9	4.9	0.06	2.4	0.69	−13.8	−116.6
6.1	0.07	49.5	0.12	2.6	13.1	0.42	2.0	6.8	0.08	0.8	1.67	−13.7	−116.6

[a]All analyte concentrations are in mg L^{-1} unless given otherwise; bd = below detection, NA = not available. Additional measurements for this visit can be found in Figures 6 and 7.

Table 2B. Summary of Concentrations of Selected Analytes From Samples Collected on 16 March 2015 From the Sediment Pore Water[a]

Depth (cm)	Ba	Ca	Fe	K	Mg	Mn	Na	Si	Sr	$NH_3 + NH_4^+$-N mg/L
0.6										11.1
1.5	0.25	78.5	0.62	4.9	17.3	1.0	2.8	20.3	0.09	
5.3										12.5
6.7	0.12	76.6	0.65	4.8	17.4	1.0	2.5	17.4	0.09	
10.5										4.7

[a]All analyte concentrations are in mg L^{-1} unless given otherwise. Additional measurements for this visit can be found in Figures 6 and 7.

consistently with depth from 9.3 to 2.3 mg g^{-1} from the top of the core to 17 cm depth (Figure 4E). Total P was low in concentration but relatively consistent with depth (average ~1.0 mg g^{-1}) until 15 cm depth when it decreased to a final concentration of 0.5 mg g^{-1} at 17 cm (Figure 4F). Values of δ^{15}N (total N; range 1.5 to 2.9‰, Figure 4D) are typical of organic N found in particulate organic matter of lacustrine systems (−5.7 to 10.6‰) [*Clark and Fritz*, 1997; *Cloern et al*., 2002]. There was an initial enrichment in δ^{34}S (total S, 5.6 to 8.6‰, Figure 4E) followed by a slow depletion and returned to a value of 5.3‰ at 17 cm depth.

4.3. Linked Sediment and Water Column Chemistry

Two sediment cores were collected on 16 March 2015 in conjunction with vertical water column sampling at GT2. One core was analyzed for geochemical parameters, while the second core was used to determine microbial composition and abundance (discussed below). In parallel with the sediment cores a pore water sampler (peeper) that had been installed about 2 weeks earlier was retrieved such that the water column chemistry could be related to the pore water composition (Figures 6 and 7). The chemocline was at about 4 m depth (Figure 6A, inset), and the CH_4 concentration increased below this level and appears to have been continuous into the sediment bed with a maximum at 4 cm depth (5.6 mM). The 4 cm depth was also the location of the peak in dissolved DIC and DOC in the pore water (Figures 6B and 6D) which is consistent with a highly bioactive anoxic zone in this layer in the sediment. The $\delta^{13}C_{DIC}$ and $\delta^{13}C_{DOC}$ became enriched with depth in the sediment pore water (Figures 6C and 6E); however, there is an apparent discontinuity with the sediment $\delta^{13}C_{DOC}$ being isotopically lighter than that of the water column. The isotopic separation between $\delta^{13}C_{DIC}$ and $\delta^{13}C_{DOC}$ ($\varepsilon_{DIC\text{-}DOC}$) can be calculated with an adaptation of the method of *Teranes and Bernasconi* [2005] using equation (2).

$$\varepsilon_{DIC-DOC} = 10^3\left\{\left[\left(\delta^{13}C_{DIC} + 1000\right)/\left(\delta^{13}C_{DOC} + 1000\right)\right] - 1\right\} \quad (2)$$

Values of $\varepsilon_{DIC\text{-}DOC}$ (Figure 6F) in the water column ranged from 22.2 to 24.5‰, while the values calculated for the sediment pore water ranged from 36 to 39‰. The significance of these differing ranges will be discussed below.

Total NH_3 began increasing in concentration below the chemocline and continued into the sediment with a maximum (12.5 mg N L^{-1}) around 4–5 cm (Figure 7A). The total S^{2-} concentration was higher near the bottom of the water column (~1.0 mg S^{2-} L^{-1}) than in the pore water (0.39 to 0.58 mg S^{2-} L^{-1}, Figure 7B).

Table 2C. Summary of Concentrations of Selected Analytes From Samples Collected on 16 March 2015 From the Analysis of Solid Sediment Material[a]

Depth (cm)	Total C mg/g	Org. C mg/g	Frac Org C	Frac Inorg C	$\delta^{13}C_{Total\ C}$	$\delta^{13}C_{Org\ C}$	$\delta^{13}C_{Inorg\ C}$
1	332	302	0.91	0.09	−26.3	−27.3	−16.6
3	434	420	0.97	0.03	−26.7	−27.0	−18.2
5	449	434	0.97	0.03	−26.4	−26.6	−21.7
7	444	277	0.62	0.38	−26.4	−26.4	−26.5
9	385	309	0.80	0.20	−26.6	−27.2	−24.0
11	384	333	0.87	0.13	−26.8	−27.4	−22.7
13	331	243	0.74	0.26	−25.7	−27.8	−19.9
15.5	332	249	0.75	0.25	−25.5	−27.7	−18.9

[a]All analyte concentrations are in mg L^{-1} unless given otherwise. Additional measurements for this visit can be found in Figures 6 and 7.

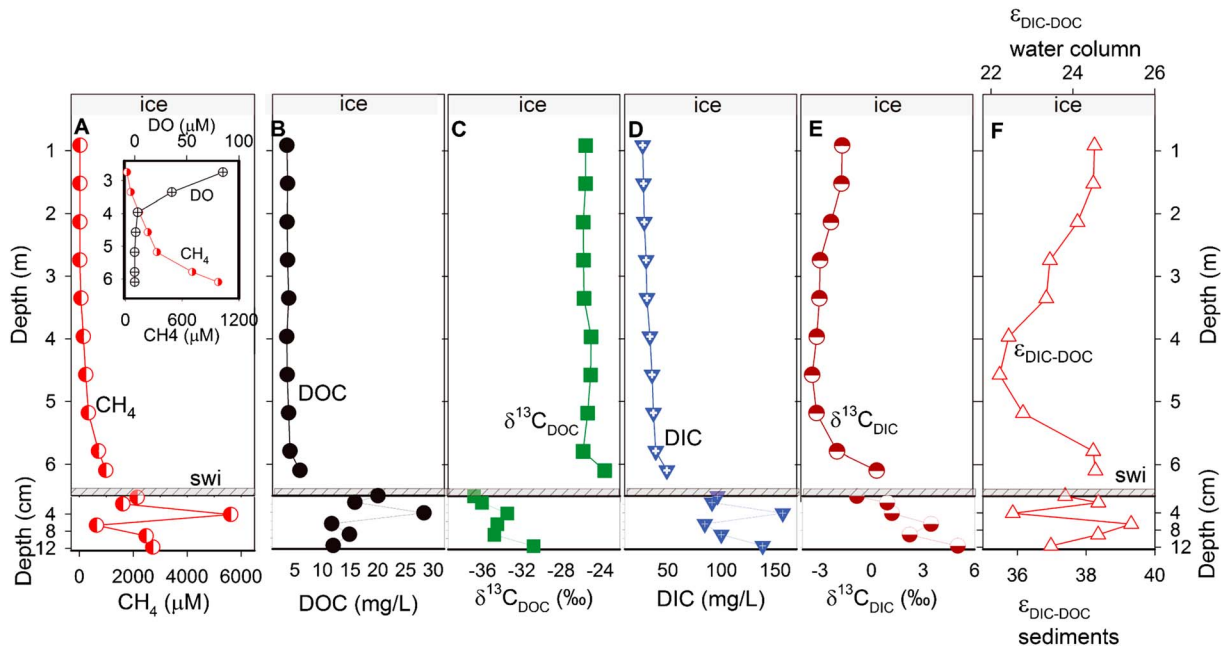

Figure 6. Water column (depth in meters) and sediment pore water (depth in centimeters) chemistry at the GT2 site, 16 March 2015 (two depth axes not to scale). (A) Dissolved CH_4 with inset showing dissolved O_2 and CH_4 defining chemocline boundary (~4 m), (B) dissolved organic carbon (DOC), (C) $\delta^{13}C_{DOC}$, (D) dissolved inorganic carbon (DIC), (E) $\delta^{13}C_{DIC}$, and (F) isotopic separation between DIC and DOC, $\varepsilon_{DIC\text{-}DOC}$ (ranges different for upper and lower panels in Figure 6F).

As shown previously, SO_4^{2-} concentration varied inversely with S^{2-}. Concentrations of Fe and Mn were both higher in the pore water than in the water column below the chemocline (Figure 7C). Additional water column and pore water profiles showing selected elemental composition as well as water isotope composition can be found in Tables 2A–2C.

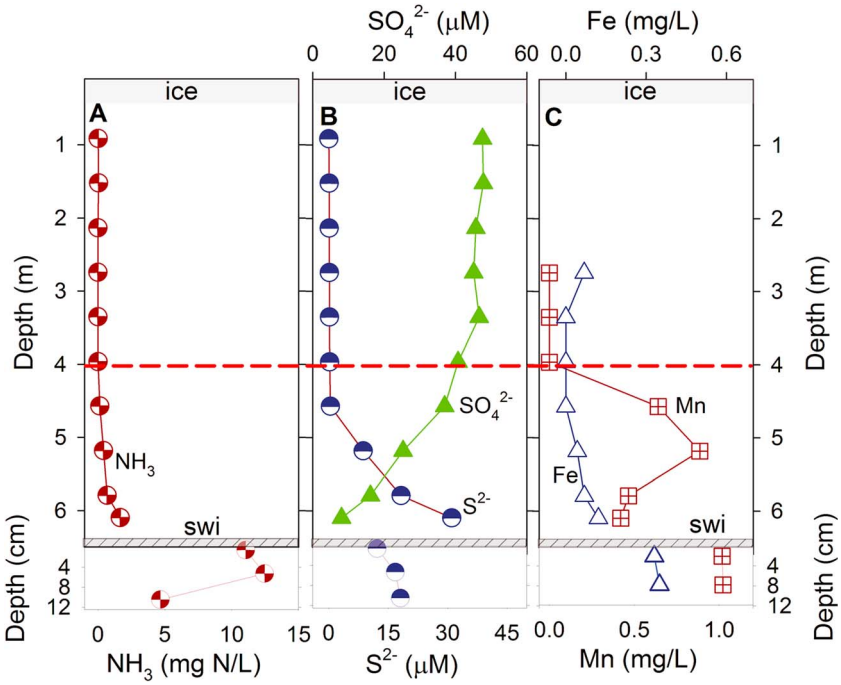

Figure 7. Water column (depth in meters) and sediment pore water (depth in centimeters) chemistry at the GT2 site, 16 March 2015 (two depth axes not to scale). (A) Dissolved total NH_3, (B) total S^{2-} in water column and sediment and dissolved SO_4^{2-} in water column, and (C) dissolved Mn and Fe concentration in water column and pore water.

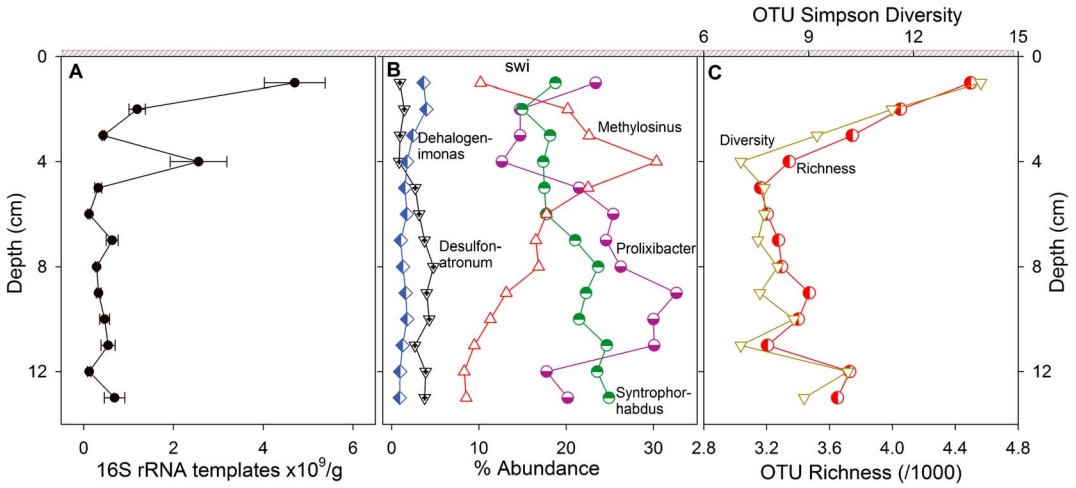

Figure 8. Sediment microbial composition as a function of depth from 16 March 2015. (A) Microbial 16S RNA templates $\times 10^9$ per gram sediment as a proxy for microbial biomass, (B) relative abundance of the five most abundant OTUs with depth, and (C) richness and Simpson Diversity based on OTU distributions. Diversity indices were calculated using PAST software.

4.4. Microbial Composition of Sediment

The second sediment core collected on March 2015 was sectioned into 1 cm interval and analyzed for the abundance and composition of 16S rRNA genes. The highest abundance of 16S rRNA templates was at the surface of the core (Figure 8A), where a total of $4.7 \times 10^9 \pm 6.8 \times 10^8$ templates g^{-1} was detected. There was a second peak in template abundance near the 4 cm depth ($2.6 \times 10^9 \pm 6.3 \times 10^8$) which coincides with the concentration maxima described above in CH_4, DIC, and DOC.

A total of 592,532 reads was obtained by multiplexed sequencing of 16S rRNA gene amplicons from the 13 sediment core depth intervals sampled, which after processing resulted in 16,030 16S rRNA gene sequences of 250 bp length per depth interval sampled. The 16S rRNA sequences were separated into operational taxonomic units (OTUs) and at a broad level; cluster analysis of these OTU profiles indicated that the 13 sediment communities could be assigned to four depth intervals: 2–4 cm, 5–8 cm, 9–11 cm, and 12–13 cm with the surface sample serving as an outgroup (supporting information Figure S3). The majority of sequences binned into five OTUs (54.5 to 73.7% of total reads) whose relative abundances varied systematically with depth (Figure 8B). These 16S rRNA gene OTUs exhibited affiliation with *Prolixibacter* (89% sequence identities), *Syntrophorhabdus* (89% sequence identities), *Methylosinus* (95% sequence identities), *Desulfonatronum* (92% sequence identities), and *Dehalogenimonas* (86% sequence identities). The 16S rRNA gene richness and diversity was highest near the surface and decreased until 4–5 cm depth after which it was relatively constant toward the bottom of the core (Figure 8C). The types of OTUs and the inferred function of the most closely related strain in relation to depth within the sediment are discussed further below.

While not particularly abundant in our sequence data set, 23 OTUs with a relative abundance of $>0.1\%$ of total sequences in a given depth interval were identified with affiliation (79–100% sequence identities) to known methanogens (supporting information Table S1). Together, these OTUs composed between 0.27 and 9.47% of the total reads in the 13 depths sampled. The combined abundance of these 23 OTUs was inversely proportional with depth (Power function $R^2 = 0.69$), which was driven primarily by a disproportionate abundance of two OTUs in the top 1 cm sample that were affiliated with *Methanobacterium* (3.86% of total sequences) and *Candidatus Methanoplasma* (4.53% of total sequences).

5. Discussion

5.1. Water Column and Sediments

Vertical profiles of physical and chemical parameters measured during ice cover at GTL have been previously discussed (pH, temperature, SC, DO, δ^{18}O-DO, δ^{13}C-DIC, sulfide, and ammonia) [*Henne*, 2011; *Gammons et al.*, 2014; *Johnston*, 2014]. The sampling events reported here include measurements of dissolved organic carbon (DOC) and $\delta^{13}C_{DOC}$ (Figures 2E, 3F, and 3G) which have not been reported previously from GTL. During the

May 2014 sampling the DOC concentration increased at the same time as DIC concentration increased in the anoxic zone (Figure 2E). As was observed by *Gammons et al*. [2014] the increase in DIC concentration below the chemocline at GTL was accompanied by an enrichment in $\delta^{13}C_{DIC}$ that was attributed to acetoclastic methanogenesis which produces isotopically depleted CH_4 and enriched DIC [*Whiticar et al*., 1986; *Whiticar*, 1999]. During the May 2014 sampling, DOC concentration and $\delta^{13}C_{DOC}$ both increased below the anoxic zone boundary. This suggests that anoxygenic photosynthetic organisms were fixing the isotopically enriched DIC into microbial organic compounds some of which were released to the surrounding water column as photosynthate or soluble organic carbon compounds (i.e., amino acids, sugars, and organic acids). *Parker et al*. [2010] reported diel changes in $\delta^{13}C_{DOC}$ in a productive, high-elevation stream, with daytime increases due to photosynthetic uptake of isotopically heavier DIC and "leaking" of associated isotopically heavier DOC to the surrounding water. Additionally, the $\delta^{13}C_{TPC}$ became initially depleted directly above the chemocline but that trend reversed below the boundary becoming enriched which is also consistent with microbial cells that are incorporating the isotopically heavier C (Figure 2G). Previous work has shown the presence of anoxygenic photosynthetic microbes across the chemoclines of stratified lakes under ice cover [*Lawrence et al*., 1978; *Overmann et al*., 1994; *Tonolla et al*., 2003; *Rogozin et al*., 2009], and anoxygenic phototrophs have been detected via molecular methods below the chemocline at GTL in samples collected in April 2013 (E.S. Boyd, unpublished results).

The simultaneous decrease in SO_4^{2-} concentration and increase in S^{2-} concentration below the chemocline (Figure 2F) are characteristic of bacterial sulfate reduction, as have been observed in other lakes [*Kosolapov et al*., 2003; *Kallistova et al*., 2006]. Removal of sulfate is an important prerequisite for accumulation of CH_4 in the anoxic zone since SO_4^{2-} tends to be a preferred oxidant when compared to CO_2 [*Lovley and Klug*, 1983] and moreover can act as an oxidant for anaerobic oxidation of CH_4 [*Herczeg*, 1988]. *Gammons et al*. [2014] observed that H_2S from the euxinic bottom water at GT2 ($\delta^{34}S_{H_2S}$ +4.8 to 8.5‰; $n = 3$) had a similar S-isotopic composition to sulfate in the shallow water ($\delta^{34}S_{SO_4^{2-}} = +9.7‰$; $n = 1$) and suggested that the total sulfur pool within the lake is being cycled between sulfate and sulfide with little isotopic separation. Total S in the sediments from May 2014 continuously decreased with depth (Figure 4E) suggesting that organic S is being diagenetically processed and returned to the lake system. These results are consistent with the increasing dissolved S^{2-} concentration in pore water with depth (Figure 7B). Similar results of generally decreasing total S concentration with depth have been found in lake sediments from the northeastern U.S. [*Mitchell et al*., 1988]. The range in $\delta^{34}S_{Total}$ of the sediments (5.3 to 8.7‰) was small and similar to that of the water column $\delta^{34}S_{H_2S}$ values reported above. Others have observed that little apparent fractionation occurs during anaerobic degradation of organic S in sediment materials [*Mekhtiyeva et al*., 1976; *Nriagu and Soon*, 1985]. The initial S-isotope enrichment at the sediment-water interface may represent a different diagenetic process acting on the freshly deposited surface sediment as compared to the more deeply buried sediment. Based on observations made on March 2015 (Figure 7B) the maximum concentrations of SO_4^{2-} in near-surface waters (47.8 μM) and that of total S^{2-} (31.0 μM) below the chemocline are similar and consistent with the hypothesis that S is being cycled within the lake and its shallow sediment [*Gammons et al*., 2014].

CH_4 concentrations measured periodically near the lake bottom at GT2 from December 2013 to March 2015 increased during ice cover and decreased during open water (Figure 9). These results are consistent with a rapid turnover of the lake after ice off in the spring which likely released a large mass of CH_4 to the atmosphere. High-methane atmospheric fluxes were observed by *Riera et al*. [1999] after release of ice cover at two lakes in Wisconsin.

The relationships between the chemistry of the water column and sediment pore water (Figures 6 and 7) help clarify the major sources of chemical species to the water column. CH_4 and total NH_3 reach the highest concentrations at 4 cm depth in the sediments (Figure 6A) such that there will be a net flux of those compounds into the water column. Additionally, ebullition is considered to be one of the major routes for CH_4 to move from sediments to the water column (or atmosphere) [*Bastviken et al*., 2004], and during several visits to GTL when bottom material was disturbed visible gas bubbles were released (supporting information Picture P12). Total S^{2-} concentrations were higher in the euxinic water column than in the sediments (Figure 7B) which is consistent with the bulk of S being recycled within the lake system with additions from decomposition of organic S-containing compounds in the sediments. It is also possible that sulfide minerals form in the sediment matrix due to the high concentration of Fe and Mn described above.

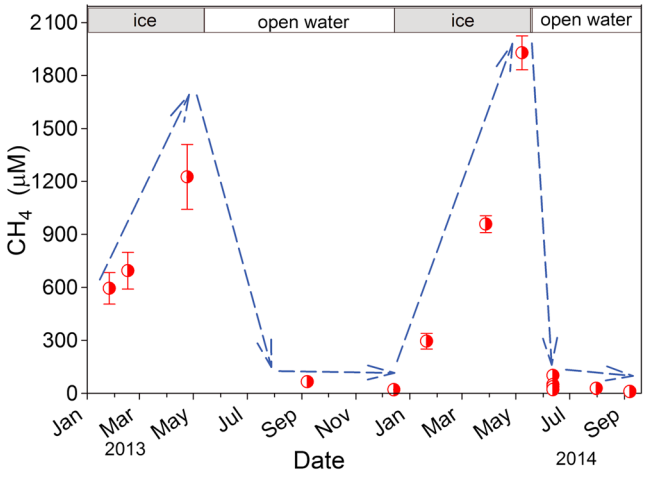

Figure 9. Methane concentration measured at the GT2 site near the sediment-water interface showing increasing concentrations under ice cover and rapid decrease after ice off. Blue dashed lines are included to approximate trends.

As described above there was a discontinuity in $\delta^{13}C_{DOC}$ across the sediment-water interface (swi) during the March 2015 sampling (Figure 6C). The magnitudes of the isotopic separation between $\delta^{13}C_{DIC}$ and $\delta^{13}C_{DOC}$ ($\varepsilon_{DIC\text{-}DOC}$, Figure 6F) in the water column were all less than 28‰ which is a characteristic of aerobic processes, while in the sediment pore water $\varepsilon_{DIC\text{-}DOC}$ values were all greater than 32‰ which is a characteristic of anaerobic microbial processes [*Teranes and Bernasconi*, 2005]. The latter observation is furthermore consistent with the presence of facultative anaerobic microbes described in the next section. The water column $\varepsilon_{DIC\text{-}DOC}$ values decreased with depth until the chemocline and then became progressively larger which underscores the increasing influence of anaerobic processes below the redox boundary (Figure 6F, upper panel). This is consistent with the increasing concentrations of Fe and Mn that were observed just below the chemocline boundary (Figure 7C) indicating that microbial communities were using electron acceptors other than O_2 such as oxidized forms of these metals as well as SO_4^{2-}. In the sediment pore water the $\varepsilon_{DIC\text{-}DOC}$ values showed an inflection at the 4 cm depth toward less isotopic separation (Figure 6F, lower panel). This zone would be expected to have very active methanogens and methanotrophs such that the cycling of C in a semiclosed compartment may result in less fractionation between organic and inorganic forms.

5.2. Microbial Sediment Composition

As shown Figure 8C the taxonomic diversity decreased through the top 4–5 cm of the sediment. This upper area also had the highest total microbial biomass (Figure 8A) and consequently was likely the most bioactive zone. This is consistent with the peak in the concentrations of DOC, DIC, and CH_4 as products of anaerobic respiration and fermentation in the upper 4 cm. This upper zone near the swi contained freshly deposited materials such as planktonic species, vascular plants, multicellular algae, and organic/inorganic particulates. Consequently, this zone may be considered the most heterogeneous in terms of available resources for microbial metabolism. Distributions of the five most abundant OTUs all showed differing patterns within the sediment profile (Figure 8B). Near the sediment surface the most abundant sequences were related (89% sequence identities) to the genus *Prolixibacter* (~20%), a known psychrotolerant facultative anaerobe that uses mixed fermentation pathways to degrade organic matter [*Holmes et al*., 2007]. The abundance of *Prolixibacter* decreased around 4 cm depth and then increased deeper within the sediment. Sequences that were related to *Methylosinus*, which had a peak in abundance at 4 cm depth (~30% of total OTUs) and showed roughly an inverse abundance relationship to *Prolixibacter*, were also detected in the sediment column. Species of the genus *Methylosinus* have been previously reported to be obligate aerobic methanotrophs [*Bowman*, 2006]. However, the O_2 concentration at 4 cm depth in the sediments should have been near zero since the DO approached zero in the water column at 4 m depth such that the bottom 2 m was anoxic and euxinic. Consequently, it is unclear to what extent the physiology of this OTU can be inferred. It is possible that the sequence related to *Methylosinus* identified in this study is derived from a strain that can tolerate anaerobic conditions and that might be capable of using electron acceptors other than O_2 (e.g., SO_4^{2-}, Mn^{4+}, and Fe^{3+}) which is consistent with the higher concentrations of Fe and Mn observed in sediment pore water (Figure 7C). The 4 cm depth had the highest concentration of dissolved CH_4, which would be consistent with this taxon being involved in methane cycling. *Syntrophorhabdus* increased in abundance with depth and is a facultative anaerobe that is known to degrade aromatic organics, perhaps originating from plant lignin transported into the lake [*Qiu et al*., 2008]. Aromatic rings are generally more recalcitrant to degradation than

nonaromatic hydrocarbons and consequently would form a larger fraction of the organic matter found with increasing depth into the sediments. *Syntrophorhabdus* is known to produce acetate as a catabolic product which then can become a substrate for acetoclastic methanogens, and some species have been shown to have a synotrophic relationship with hydrogenotrophic methanogens [*Qiu et al*., 2008]. Importantly, none of the OTUs that were affiliated with methanogens covaried with the abundance of OTUs affiliated with *Syntrophorhabdus*.

Sequences related to methanogens exhibited elevated abundance in the upper 4 cm of the sediment column (1.2 to 9.5% of total reads) when compared to deeper depth intervals (0.3 to 1.3% of total reads), consistent with higher methane concentrations in the upper 4 cm interval. The most abundant methanogen exhibited distant affiliation (86% sequence identities) with *Candidatus Methanoplasma*, which belongs to a newly described order of methanogens that produce methane through the hydrogen-dependent reduction of methanol or methylamines [*Lang et al*., 2015]. Such substrates might be made available through the anaerobic degradation of lignin and plant-derived or microbial-derived biomass. Interestingly, the distribution of this taxon was largely concentrated in the top 1 cm of the sediment column, while the highest pore water CH_4 concentrations were identified at 4 cm depth. That said, a small bump in pore water CH_4 was observed at the swi which might be due to the activity of this organism. A second taxon, related to methanogens, showed close affiliation (98% sequence identities) to *Methanobacterium*, an organism that can produce CH_4 via hydrogenotrophic pathways [*Zellner et al*., 1988]. The abundance of this taxon was also highest in the top 1 cm of sediment (3.86% of total sequences). However, unlike *C. Methanoplasma*, the abundance of this taxon was also elevated in the 2 to 4 cm depth interval (0.62–0.74% of the sequences) but not in the 5 to 13 cm depth intervals (0.0 to 0.1% of total sequences). Additional and more targeted sequencing (e.g., metagenomics and targeted functional gene work) is needed to pin down the role of methanogen populations and their specific metabolisms in contributing to CH_4 cycling in the sediments at GTL.

The genus *Desulfonatronum* displayed a relatively constant abundance with depth and is a known sulfate-reducing bacterium [*Pikuta et al*., 2003; *Zhilina et al*., 2005], using electron donors such as acetate [*Wetzel*, 2001]. This suggests that low concentrations of SO_4^{2-}, as an electron acceptor, must be present within the sediment column. *Dehalogenimonas* was also relatively constant in abundance with depth and is known to use hydrogen as an electron donor in conjunction with the dehalogenation of alkanes [*Moe et al*., 2009]. This is an interesting genus to be found in this setting since other members have been identified in groundwater contaminated with halogenated hydrocarbons [*Bowman et al*., 2013], but this study did not attempt to detect these types of halogenated compounds. It is important to note that many of the OTUs discussed above exhibit fairly low sequence identities to cultivars, which may obfuscate our ability to infer physiology based on phylogenetic relationships. Ongoing work is aimed at using genomic methods to further characterize the physiologic capabilities of these OTUs.

5.3. Carbon Diagenesis

As previously described (Figures 4 and 5) there was a relatively consistent decrease in the total C content with depth in the sediment cores at each site presumably due to microbial degradation of organic carbon ultimately resulting in the formation of CO_2 and CH_4. In order to quantify the return of C from lake sediments to the water column (and atmosphere, C turnover), the cores from July 2014 were used to determine the decrease in the mass of total C with depth into the sediment as a function of time. The sediment cores collected at GTL typically ended near the deepest part of the core with a clay-rich layer filled with small rocks, and this layer was presumed to be the prereservoir floodplain (about 130 yr B.P.). Since age dating of sediment material was not performed, it was assumed that the mass accumulation rate has been relatively constant over time which made it possible to assign an approximate age with depth to the segments analyzed from each core. Based on the dry mass and dimensions of the core segments, it was calculated that the C turnover rates (decrease in total C) were 1.1×10^2, 2.5×10^2, and 5.8×10^2 g m^{-2} yr^{-1} at RB1, SM1 and GT2, respectively. GTL has a surface area of 1220 ha [*Knight*, 1981] and is a shallow lake without a significant amount of bottom contour. Assuming that about one third of the lake is deep enough to have accumulated enough C to contribute significantly to CO_2 and CH_4 production, this translates to a bottom surface area of about 4.1×10^6 m^2. Using an average of the C turnover rates from the three sites, GTL may be releasing as much as 1.3×10^9 g C yr^{-1} (1.1×10^8 mol yr^{-1}) from the sediments to lake waters and the atmosphere. Some of the newly mobilized C is presumably

retained in the sediments by carbonate mineralization (e.g., $CaCO_3$ and $FeCO_3$); however, this calculation is based on the decrease in total C with depth across the core. *Fahrner et al*. [2008] estimated a total C production from anaerobic respiration of 4.8×10^8 g yr^{-1} from the hypolimnion of a eutrophic maar lake in Germany. *Michmerhuizen et al*. [1996] estimated that as much as 1.5×10^9 g of C was emitted by all Minnesota lakes north of the 45 parallel in 1 year. *Johnston* [2014] calculated that as much as 1.2×10^9 mol (1.9×10^{10} g) of CH_4 could be released from GTL to the atmosphere at spring turnover. This latter calculation was based only on CH_4 concentrations observed at GT2 from one season, while the above determination used total C values recorded at three separate sites in the sediment bed for a ~130 year period. However, both estimates suggest that large amounts of C are potentially being returned to the atmosphere as greenhouse gases. Additionally, *Johnston* [2014] calculated that methanotrophic soil microbes within the GTL watershed could consume approximately 1.6×10^8 g C yr^{-1}, several orders of magnitude less than that being released to the atmosphere.

The above calculations are limited by the assumption that the C accumulation rate has been constant but still serves to underscore the significance of freshwater lakes as sources of greenhouse gases. *Michmerhuizen et al*. [1996] estimated that as much as 40% of all CH_4 discharged to the atmosphere annually may come from springtime releases of small, temperate climate lakes.

6. Summary

We have described seasonal and spatial changes in water column and sediment pore water chemistry and stable isotope compositions of various chemical species. Additionally, the microbial composition of the lake bed sediments has been examined and related to the composition of the surrounding pore water. The largest abundance of putative methanotrophs (*Methyosinus*) was shown to occur at the same depth in the sediment core as the maximum in CH_4 concentration. Methane concentrations decreased systematically toward the sediment-water interface possibly due to the activity of this strain in conjunction with diffusion/ebullition into the water column. It is possible that the sequence affiliated with *Methylosinus* corresponded to a variant since type strains of *Methylosinus* are obligate aerobes, and oxygen was not present in high abundances in the sediment. Intriguingly, the abundance of putative methanogens was highest near the swi, which may suggest the presence of a dynamic CH_4 cycling community in GTL. *Prolixibacter* was the most abundant organism in the sediment surface, which is consistent with its role in anaerobic breakdown of organic matter. A comparison of stable isotopes of DIC and DOC in the sediment pore water ($\varepsilon_{DIC\text{-}DOC}$) is consistent with anaerobic microbial processes influencing the sediment ecosystem. Whereas the entire water column of the lake becomes aerated during summer months, the sediment likely remains anoxic due to high rates of respiration consuming O_2 rapidly as it diffuses into the sediment pore water.

Enrichment of $\delta^{13}C_{DOC}$ below the chemocline under ice cover suggests that anoxygenic photosynthetic microbes are present in that region and that enough light is penetrating the ice/snow cover to provide an energy source for those organisms. This is consistent with our unpublished data from water column samples collected under ice cover which indicated that anoxygenic phototrophs are dominant below the chemocline. N-stable isotopes of the sediments are typical of organic N and that decomposition of this organic N is an important source of reduced N species to the water column. S-stable isotopes in the sediments were similar in range to those reported previously for water column species in GTL. This is consistent with a large degree of internal cycling of S within the lake. Concentrations of S in the sediments decreased with depth indicating breakdown of organic S-containing compounds forming reduced S species (sulfides).

Our estimates of the rate of degradation of organic carbon based on the rate of C decrease within the sediment column of Georgetown Lake are in the same range as those calculated for other temperate climate freshwater lakes. The ultimate breakdown products of anaerobic fermentation of organic biomass are CO_2 and CH_4. Evidence presented in this manuscript indicates that GTL most likely produces a net flux of CH_4 to the atmosphere each spring and through ebullition throughout the ice-free season.

Acknowledgments
We thank J. Timmer for analytical assistance and L. Johnston for field assistance. Thanks to R. West Sr. for the gracious use of his boat. This work was funded in part by grants from the Montana Institute on Ecosystems and the National Science Foundation (0739054, 1338040). The NASA Astrobiology Institute is supported by grant NNA15BB02A. Funding for J. Feyhl-Buska was provided in part by the MSU Undergraduate Scholars Program. All data generated as part of this project are included in figures, tables, and text within this manuscript or in the supporting information. This manuscript has been greatly improved by the comments of two anonymous reviewers.

References

Bastviken, D., L. J. Tranvik, J. A. Downing, P. M. Crill, and A. Enrich-Prast (2011), Freshwater methane emissions offset the continental carbon sink, *Science*, *331*, 50.

Bastviken, D. J., J. Cole, M. Pace, and L. Tranvik (2004), Methane emissions from lakes: Dependence of lake characteristics, two regional assessments, and a global estimate, *Global Biogeochem. Cycles*, *18*, GB4009, doi:10.1029/2004GB002238.

Borg, H., and P. Jonsson (1996), Large-scale metal distribution in Baltic Sea sediments, *Mar. Pollut. Bull.*, *12*(1), 8–12.
Bowman, J. (2006), The methanotrophs—The families Methlyococcaceae and Methylocystaceae, *Prokaryotes*, *5*, 266–289.
Bowman, K. S., M. F. Nobre, M. S. da Costa, F. A. Rainey, and W. M. Moe (2013), Dehalogenimonas alkenigignens sp. nov., a chlorinated-alkane-dehalogenating bacterium isolated from groundwater, *Int. J. Syst. Evol. Microbiol.*, *63*(4), 1492–8, doi:10.1099/ijs.0.045054-0.
Boyd, E. S., R. A. Jackson, G. Encarnacion, J. A. Zahn, T. Beard, W. D. Leavitt, Y. Pi, C. L. Zhang, A. Pearson, and G. G. Geesey (2007), Isolation, characterization, and ecology of sulfur-respiring Crenarchaea inhabiting acid-sulfate-chloride-containing geothermal springs in Yellowstone National Park, *Appl. Environ. Microbiol.*, *73*, 6669–6677.
Boyd, E. S., R. K. Lange, A. C. Mitchell, J. R. Havig, T. L. Hamilton, M. J. Lafreniere, E. L. Shock, J. W. Peters, and M. Skidmore (2011), Diversity, abundance, and potential activity of nitrifying and nitrate-reducing microbial assemblages in a subglacial ecosystem, *Appl. Environ. Microbiol.*, *77*, 4778–4787.
Clark, I. D., and P. Fritz (1997), *Environmental Isotopes in Hydrogeology*, Lewis Publ., New York.
Cloern, J. E., E. A. Canuel, and D. Harris (2002), Stable carbon and nitrogen isotope composition of aquatic and terrestrial plants of the San Francisco Bay estuarine system, *Limnol. Oceanogr.*, *47*(3), 713–729.
Downing, J. A., et al. (2006), The global abundance and size distribution of lakes, ponds, and impoundments, *Limnol. Oceanogr.*, *51*, 2388–2397.
Downing, J. A., J. J. Cole, J. J. Middelburg, R. G. Striegl, C. M. Duarte, P. Kortelainen, Y. T. Prairie, and K. A. Laube (2008), Sediment organic carbon burial in agriculturally eutrophic impoundments over the last century, *Global Biogeochem. Cycles*, *22*, GB1018, doi:10.1029/2006GB002854.
Edgar, R. C., B. J. Haas, J. C. Clemente, C. Quince, and R. Knight (2011), UCHIME improves sensitivity and speed of chimera detection, *Bioinformatics*, *27*, 2194–2200.
Einsele, G., J. Yan, and M. Hinderer (2001), Atmospheric carbon burial in modern lake basins and its significance for the global carbon budget, *Global Planet. Change*, *30*, 167–195.
Fahrner, S., M. Radke, D. Karger, and C. Blodau (2008), Organic matter mineralisation in the hypolimnion of an eutrophic Maar lake, *Aquat. Sci.*, *70*, 225–237.
Gammons, C. H., W. Henne, S. R. Poulson, S. R. Parker, T. B. Johnston, J. E. Dore, and E. S. Boyd (2014), Stable isotopes track biogeochemical processes under seasonal ice cover in a shallow, productive lake, *Biogeochemistry*, *120*, 359–379, doi:10.1007/s10533-014-0005-z.
Garrett, P. A. (1983), Relationships between benthic communities, land use, chemical dynamics, and trophic state in Georgetown Lake, PhD Dissertation, Montana State Univ., Bozeman, Montana.
Gaudino, S., C. Galas, M. Belli, S. Barbizzi, P. de Zorzi, R. Jacimovic, Z. Jeran, A. Pati, and U. Sansone (2007), The role of different soil sample digestion methods on trace elements analysis: A comparison of ICP-MS and INAA measurement results, *Accred. Qual. Assur.*, *12*, 84–93.
Giesemann, A., H. J. Jager, A. L. Norman, H. P. Krouse, and W. A. Brand (1994), On-line sulfur-isotope determination using an elemental analyzer coupled to a mass spectrometer, *Anal. Chem.*, *66*, 2816–2819.
Grassineau, N. V., D. P. Mattey, and D. Lowry (2001), Sulfur isotope analysis of sulfide and sulfate minerals by continuous flow-isotope ratio mass spectrometry, *Anal. Chem.*, *73*, 220–225.
Hamilton, T. L., J. W. Peters, M. L. Skidmore, and E. S. Boyd (2013), Molecular evidence for an active endogenous microbiome beneath glacial ice, *ISME J.*, *7*, 1402–1412.
Hammer, Ø., D. A. T. Harper, and P. D. Ryan (2001), PAST: Paleontological statistics software package for education and data analysis, *Palaeontol. Electron.*, *4*(1).
Henne, W. (2011), Using chemical and isotopic tracers to track biogeochemical processes under ice cover at Georgetown Lake, Montana, MS Thesis, Montana Tech of The Univ. of Montana, Butte, Montana.
Herczeg, A. L. (1988), Early diagenesis of organic matter in lake sediments: A stable carbon isotope study of pore waters, *Chem. Geol.*, *72*, 199–209.
Hesslein, R. H. (1976), An in situ sampler for close interval pore water studies, *Limnol. Oceanogr.*, *21*, 912–914.
Holmes, D. E., K. P. Nevin, T. L. Woodard, A. D. Peacock, and D. R. Lovley (2007), Prolixibacter bellariivorans gen. nov., sp. nov., a sugar-fermenting, psychrotolerant anaerobe of the phylum Bacteroidetes, isolated from a marine-sediment fuel cell, *Int. J. Syst. Evol. Microbiol.*, *57*, 701–707, doi:10.1099/ijs.0.64296-0.
Johnston, T. B. (2014), Methanogenesis, redox and carbon isotope biogeochemistry: Georgetown Lake, Montana, MS Thesis, Montana Tech, Butte, Montana.
Jones, J. B., and J. P. Mulholland (2000), *Streams and Ground Waters*, Academic Press, San Diego, Calif.
Kallistova, A. Y., M. V. Kevbrina, N. V. Pimenov, I. I. Rusanov, D. Y. Rogozin, B. Wehrli, and A. N. Nozhevnikova (2006), Sulfate reduction and methanogenesis in the Shira and Shunet Meromictic Lakes (Khakasia, Russia), *Microbiology*, *75*(6), 720–726.
Kastowski, M., M. Hinderer, and A. Vecsei (2011), Long-term carbon burial in European lakes: Analysis and estimate, *Global Biogeochem. Cycles*, *25*, GB3019, doi:10.1029/2010GB003874.
Knight, J. C. (1981), An investigation of the general limnology of Georgetown Lake, Montana, PhD Dissertation, Montana State Univ., Bozeman, Montana.
Knight, J. C., P. J. Garrison, and J. C. Wright (1976), An investigation into the extent and cause of eutrophication in Georgetown Lake, Montana, Montana Univ. Joint Water Resour. Res. Cent., Bozeman, Montana, Rep. 77.
Kosolapov, D. B., D. Y. Rogozin, I. A. Gladchenko, A. I. Kopylov, and E. E. Zakharova (2003), Microbial sulfate reduction in a brackish meromictic steppe lake, *Aquat. Ecol.*, *37*, 215–226.
Lang, K., J. Schuldes, A. Kling, A. Poehlein, R. Daniel, and A. Brune (2015), New mode of energy metabolism in the seventh order of methanogens as revealed by comparative genome analysis of "Candidatus Methanoplasma termitum", *Appl. Environ. Microbiol.*, *81*(4), 1338–1352, doi:10.1128/AEM.03389-14.
Lawrence, J. R., R. C. Haynes, and U. T. Hammer (1978), Contribution of green photosynthetic bacteria to total primary production in a meromictic saline lake, *Verh. Int. Ver. Limnol.*, *20*, 201–207.
Lewis, E., and D. W. R. Wallace (1998), Program developed for CO_2 system calculations, ORNL/CDIAC-105, Carbon dioxide information analysis center, Oak Ridge Nat. Lab., U.S. Department of Energy, Oak Ridge, Tenn. [Availabe at http://cdiac.ornl.gov/oceans/co2rprt.html, accessed 15-Oct. 2015.]
Lovley, D. R., and M. J. Klug (1983), Sulfate reducers can outcompete methanogens at freshwater sulfate concentrations, *Appl. Environ. Microbiol.*, *45*(1), 187–192.
Mekhtiyeva, V. L., R. G. Pankina, and Y. Y. Gavrilov (1976), Distributions and isotopic composition of forms of sulfur in water animals and plants, *Geochem. Int.*, *13*, 82–87.
Michmerhuizen, C. M., R. G. Striegl, and M. E. McDonald (1996), Potential methane emission from north temperate lakes following ice melt, *Limnol. Oceanogr.*, *41*, 985–991.

Mitchell, M. J., S. C. Schindler, J. S. Owen, and S. A. Norton (1988), Comparison of sulfur concentrations within lake sediment profiles, *Hydrobiologia*, *157*, 219–229.

Moe, W. M., J. Yan, M. F. Nobre, M. S. Da Costa, and F. A. Rainey (2009), Dehalogenimonas lykanthroporepellens gen. nov., sp. nov., a reductively dehalogenating bacterium isolated from chlorinated solvent-contaminated groundwater, *Int. J. System. Evol. Microbiol.*, *59*(11), 2692–2697, doi:10.1099/ijs.0.011502-0.

Moss, B., et al. (2011), Allied attack: Climate change and eutrophication, *Inland Waters*, *1*, 101–105.

Nriagu, J. O., and Y. K. Soon (1985), Distribution and isotopic composition of sulfur in lake sediments of northern Ontario, *Geochim. Cosmochim. Acta*, *49*, 823–834.

Overmann, J. J., T. Beatty, and K. J. Hall (1994), Photo-synthetic activity and population dynamics of *Amoebobacter purpureus* in a meromictic saline lake, *Fed. Eur. Microbial. Sot. Microbial. Ecol.*, *15*, 309–320.

Parker, S. R., S. R. Poulson, C. L. Weyer, M. G. Smith, and K. N. Bates (2010), Temporal variability in the concentration and stable carbon isotope composition of dissolved inorganic and organic carbon in streams, *Aquat. Geochem.*, *16*, 61–84, doi:10.1007/s10498-009-9068-1.

Pikuta, E. V., R. B. Hoover, A. K. Bej, D. Marsic, W. B. Whitman, D. Cleland, and P. Krader (2003), Desulfonatronum thiodismutans sp. nov., a novel alkaliphilic, sulfate-reducing bacterium capable of lithoautotrophic growth, *Int. J. Syst. Evol. Microbiol.*, *53*(5), 1327–1332.

Qiu, Y., S. Hanada, A. Ohashi, H. Harada, Y. Kamagata, and Y. Sekiguchi (2008), *Syntrophorhabdus aromaticivorans* gen. nov., sp. nov., the first cultured anaerobe capable of degrading phenol to acetate in obligate syntrophic associations with a hydrogenotrophic methanogen, *Appl. Environ. Microbiol.*, *74*(7), 2051–2058, doi:10.1128/AEM.02378-07.

Riera, J. L., J. E. Shindler, and T. K. Kratz (1999), Seasonal dynamics of carbon dioxide and methane in two clear-water lakes and two bog lakes in northern Wisconsin, U.S.A., *Can. J. Fish. Aquat. Sci.*, *56*, 265–274.

Rodhe, H. (1990), A comparison of the contribution of various gases to the greenhouse effect, *Science*, *248*, 1217–1219.

Rogozin, D. Y., V. V. Zykov, M. Y. Chernetskii, and A. G. Degermendzhy (2009), Anoxygenic phototrophic bacteria in meromictic lakes of southern Siberia during the ice period: Spatial distributions and ecological conditions, *Doklady Biol. Sci.*, *424*(1), 63–67.

Rudd, J. W. M., and R. D. Hamilton (1978), Methane cycling in a eutrophic shield lake and its effect on whole lake metabolism, *Limnol. Oceanogr.*, *23*, 337–348.

Scheffer, M., S. Carpenter, J. A. Foley, C. Folke, and B. Walker (2001), Catastrophic shifts in ecosystems, *Nature*, *413*, 591–596.

Schloss, P. D., et al. (2009), Introducing mothur: Open-source, platform-independent, community-supported software for describing and comparing microbial communities, *Appl. Environ. Microbiol.*, *75*, 7537–7541.

Schubert, C. J., T. Diem, and W. Eugster (2012), Methane emissions from a small wind-shielded lake determined by eddy covariance, flux chambers, anchored funnels, and boundary model calculations: A comparison, *Environ. Sci. Technol.*, *46*, 4515–4522.

Shaw, G. D., E. S. White, and C. H. Gammons (2013), Characterizing groundwater–lake interactions and its impact on lake water quality, *J. Hydrol.*, *49*, 69–78.

Smith, V. H., and D. W. Schindler (2009), Eutrophication science: Where do we go from here?, *Trends Ecol. Evol.*, *24*(4), 201–207.

Stafford, C. P. (2013), Long-term trends in the water quality of Georgetown Lake, Montana, Prepared for Mont Dept. Justice and Mont. Dept. Environ. Quality, 126 pp.

Stumm, W., and J. J. Morgan (1996), *Aquatic Chemistry*, Wiley-Interscience, New York.

Tamura, K., G. Stecher, D. Peterson, A. Filipski, and S. Kumar (2013), MEGA6: Molecular Evolutionary Genetics Analysis Version 6.0, *Mol. Biol. Evol.*, *30*(12), 2725–2729.

Teranes, J. L., and S. M. Bernasconi (2005), Factors controlling $\delta^{13}C$ values of sedimentary carbon in hypertrophic Baldeggersee, Switzerland, and implications for interpreting isotope excursions in lake sedimentary records, *Limnol. Oceanogr.*, *50*, 914–922.

Tonolla, M., S. Peduzzi, D. Hahn, and R. Peduzzi (2003), Spatio-temporal distribution of phototrophic sulfur bacteria in the chemocline of meromictic Lake Cadagno (Switzerland), *FEMS Microbiol. Ecol.*, *43*, 89–98.

Trabert, M. J. (1993), The depletion of oxygen in Georgetown Lake, Montana, during the winter months. MS Thesis, Montana Tech.

Tranvik, L. J., et al. (2009), Lakes and reservoirs as regulators of carbon cycling and climate, *Limnol. Oceanogr.*, *54*, 2298–2314.

U.S. Environmental Protection Agency (EPA) (1976), Preliminary Report on Georgetown Lake, National Eutrophication Survey, CERL. Corvallis, OR, 27 pp.

Utsumi, M., Y. Nojiri, T. Nakamura, T. Nozawa, A. Otsuki, and H. Seki (1998), Oxidation of dissolved methane in a eutrophic, shallow lake: Lake Kasumigaura, Japan, *Limnol. Oceanogr.*, *43*, 471–480.

Werner, R. A., B. A. Bruch, and W. A. Brand (1999), ConFlo III—An interface for high precision $\delta^{13}C$ and $\delta^{15}N$ analysis with an extended dynamic range, *Rapid Commun. Mass Spectrom.*, *13*, 1237–1241.

Wetzel, R. G. (2001), *Limnology: Lake and River Ecosystems*, 3rd ed., Academic Press, San Diego, Calif.

Whiticar, M. J. (1999), Carbon and hydrogen isotope systematics of bacterial formation and oxidation of methane, *Chem. Geol.*, *161*, 291–314.

Whiticar, M. J., E. Faber, and M. Schoell (1986), Biogenic methane formation in marine and freshwater environments: CO_2 reduction vs. acetate fermentation—Isotope evidence, *Geochim. Cosmochim. Acta*, *50*, 693–709.

Wiesenburg, D. A., and N. L. Guinasso Jr. (1979), Equilibrium solubilities of methane, carbon monoxide and hydrogen in water and sea water, *J. Chem Eng. Data*, *24*(4), 356–360.

Zellner, G., K. Bleicher, E. Braun, H. Kneifel, B. J. Tindall, E. Conway de Macario, and J. Winter (1988), Characterization of a new mesophilic, secondary alcohol-utilizing methanogen, Methanobacterium palustre spec. nov. from a peat bog, *Archives Microbiol.*, *151*(1), 1–9.

Zhilina, T. N., D. G. Zavarzina, J. Kuever, A. M. Lysenko, and G. A. Zavarzin (2005), Desulfonatronum cooperativum sp. nov., a novel hydrogenotrophic, alkaliphilic, sulfate-reducing bacterium, from a syntrophic culture growing on acetate, *Int. J. Syst. Evol. Microbiol.*, *55*(3), 1001–1006.